Available online at www.sciencedirect.com
SCIENCE DIRECT®
Catalysis Today 107–108 (2005) 849–855
CATALYSIS TODAY
www.elsevier.com/locate/cattod

# XANES study of electronic and structural nature of Mn-sites in manganese oxides with catalytic properties

Santiago J.A. Figueroa [a], Félix G. Requejo [a], E.J. Lede [a], Luciano Lamaita [b], M. Andrés Peluso [b], Jorge E. Sambeth [b,*]

[a] Dto. Física, FCE, UNLP, IFLP e INIFTA (CONICET) c.c. 67. 1900 La Plata, Argentina
[b] Centro de Investigación y Desarrollo en Ciencias Aplicadas "Dr. Jorge J. Ronco" CINDECA (UNLP-CONICET) 47 Nro. 257, cc 59 (B1900AJK) La Plata, Argentina

Available online 24 August 2005

**Abstract**

The characterization of a series of manganese oxides prepared by different methods were performed by X-ray diffraction (XRD) and X-ray absorption near-edge structure (XANES) analysis. Low crystallized phases were found by means of XRD. The XANES results indicated that the mean oxidation state value of all the samples was between 3+ and 4+. XANES analysis of spectra and extended X-ray absorption fine structure (EXAFS) data revealed that Mn was present in three different octahedral environments; one of them corresponded to the environment of Mn in the pyrolusite phase while the other two can be associated to Mn in ramsdellite-like environment and Mn in a octahedral site with Mn-vacancies in the second shell of coordination. The different oxides were analyzed in the reaction of total oxidation of ethanol and we found that the catalytic activity was enhanced when the couple $Mn^{3+}$–$Mn^{4+}$ was present in the structure of the oxides.


*Keywords:* XANES; PCA; Pyrolusite; Mn-vacancies

## 1. Introduction

The manganese oxides, including $MnO_2$, $Mn_2O_3$ and $Mn_3O_4$ were used in some environmental catalysis reactions for the selective reduction of $NO_x$ and CO [1,2], oxidation of volatile organic compounds (VOC's) [3–5] and elimination of organoclorates [6,7]. $MnO_2$ has been reported to be among the most efficient manganese oxides for catalytic elimination of pollutants [8]. Nevertheless, there are many $MnO_2$ polymorphs. The tetragonal pyrolusite (β-$MnO_2$) and the orthorombic ramsdellite are two of them. As we can see in Fig. 1, they form a three-dimensional network of edge and corner-sharing $MnO_6$ octahedral arranged in simple chains (pyrolusite) or double chains (ramsdellite) [9]. The nsutite (γ-$MnO_2$) is formed by the intergrowth of domains of pyrolusite and ramsdellite. Furthermore, this oxide is present in a non-stoichiometric way with $Mn^{4+}$ vacancies, $Mn^{3+}$ replacing $Mn^{4+}$ cations and $OH^-$ species replacing $O^{2-}$ anions [10]. These characteristics make this oxide interesting from the catalytic and electrochemical point of view, due to their elevated electrical conductivity. These features were pointed out by Lahouse et al. [11], who have reported that among the different $MnO_2$ phases, γ-$MnO_2$ has the best catalytic properties in the oxidation of VOCs. The authors explained the high activity of this phase by the presence of Mn vacancies. Recently, we have shown [3] that a non-stoichiometric manganese oxide containing the $Mn^{3+}$–$Mn^{4+}$ couple is more active in the oxidation of ethanol than $Mn_2O_3$ oxide. On the other hand, these characteristics of the γ-$MnO_2$ make this oxide difficult to characterize by means of common X-ray diffraction (XRD) techniques [9]. To get a better characterization of the local environment of manganese oxides, we performed X-ray absorption fine structure (XAFS) spectroscopy experiments, already established as a very accomplished method for this purpose [12–14].

Given the catalytic interest of Mn-oxide phase, like in the destruction of VOC's, our objective in this work is to

* Corresponding author. Tel.: +54 221 4211353; fax: +54 221 4214277.
*E-mail address:* sambeth@quimica.unlp.edu.ar (J.E. Sambeth).

0920-5861/$ – see front matter 
doi:10.1016/j.cattod.2005.07.156

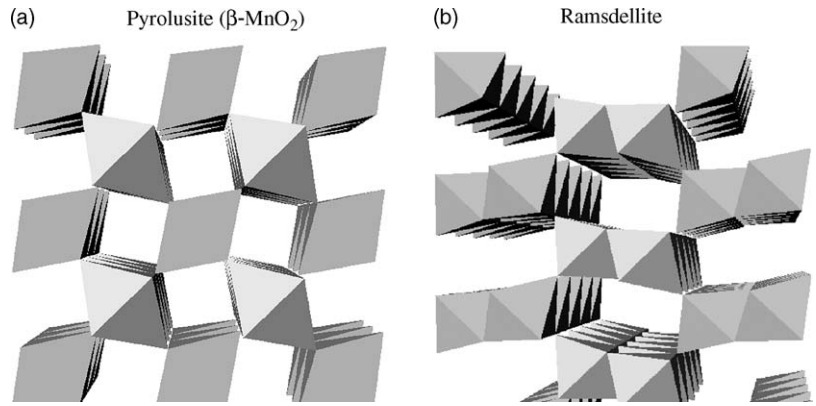


Fig. 1. The structure of: (a) pyrolusite (β-$MnO_2$) and (b) ramsdellite.

characterize, by adequate methods (XRD, XAFS), the nature of Mn-sites, including the catalytically active ones, in the different phases for the synthesized manganese oxides.

## 2. Experimental

### 2.1. Sample preparation

The preparation of the catalysts used in this work is explained in Table 1.

### 2.2. Characterization

The X Ray diffraction patterns were carried out at room temperature with a Phillips PW 1390 instrument by using Ni filter and Cu Kα radiation (λ = 1.540589 Å) in the 2$\theta$ range between 5° and 60°. For phase identification purposes, JCPDS database of reference compounds was used [15].

The BET specific surface areas were measured by $N_2$ adsorption at the liquid nitrogen temperature (77 K) in a Micromeritics Accussorb 2100 D sorptometer.

### 2.3. XANES

The XAFS experiments (including X-ray absorption near-edge structure region—XANES and extended X-ray absorption fine structure region—EXAFS) were performed at the LNLS facility by using the D04B-XAS1 beam line. The Mn K-edge spectra were collected in transmission mode using a Si(1 1 1) single channel-cut crystal monochromator at room conditions with a slit aperture of 0.5 mm, to obtain an energy resolution of about 1 eV [16]. The three ion chambers as detectors were filled with air at atmospheric pressure. The energy calibration was obtained by simultaneous absorption measurements on the Mn metal sample positioned between the second and the third ionization chamber. X-ray absorption data were analyzed by using standards procedures [17]: a linear background was fitted at the pre-edge region and then subtracted from the entire spectrum; the jump of the spectrum was normalized to unity with the post-edge asymptotic value by using a quadratic fit. The atomic background, $\mu_0(k)$, was determined by using cubic splines and the radial distribution function FT($\chi(k)$) was obtained by Fourier transforming the $k^2$ weighted experimental XAFS $\chi(k)$ function in the region of 2–15 $Å^{-1}$, multiplied by a Hanning window, into the $R$ space.

To obtain the mean oxidation state of the metal in each sample, the energy shift of the edge relative to the metal reference compound was determined by the second inflection point at the edge position of the XANES spectra [18]. In order to identify the different Mn-species from the set of measured Mn-oxides samples the principal component analysis (PCA) [19] was carried out by using a program

Table 1
Notation and BET surface area of the manganese samples used in this work

| Sample | Method of preparation | $S_{BET}$ ($m^2\,g^{-1}$) |
|---|---|---|
| β-$MnO_2$ | Commercial $MnO_2$ (Baker 99%). | 6.1 |
| $Mn_2O_3$ | Synthetic $Mn_2O_3$ obtained by decomposition of $MnCO_3$ at 700 °C [3]. | 11.6 |
| g-$MnO_2$ | Oxidation with flowing oxygen (30 $cm^3\,min^{-1}$) of a $MnSO_4$ dissolved in 3 M $H_2SO_4$. pH was raising up to 3 with NaOH. After filtration and washed with deionised water, the oxide was dried at 100 °C for 24 h [15]. | 101.0 |
| MnK | Reaction at room temperature between $Mn(NO_3)_2$ and $KMnO_4$. The permanganate solution was added to the manganese nitrate solution [16]. | 82.3 |
| KMn | Reaction at room temperature between $Mn(NO_3)_2$ and $KMnO_4$. The manganese nitrate solution was added to the permanganate solution. | 68.5 |
| EMD-st | Electrochemically deposited manganese dioxide (EMD) prepared by electrolysis at 60 °C of acidic solution of $MnSO_4$ using Ti as an anode and a stainless steel cathode [16]. | 176 |
| EMD-al | EMD prepared by electrolysis at 60 °C of acidic solution of $MnSO_4$ using Ti as an anode and aluminum as a cathode. | 170 |

developed by Fernández-García et al. [20]. The PCA method consists of a statistical methodology developed by Malinowsky [23] than can be applied on a set of normalized/energy calibrated spectra [19,20]. It can be used when the variable under study, like absorbance in a set of XANES spectra, can be represented mathematically as a linear sum of uncorrelated components (called factors), provided that the number of spectra is larger than that of the components. An important property of this method lies in the fact that every factor makes a maximum contribution to the sum of the variances of the variable.

The method utilizes the specific characteristics of the XANES region in systems with mixtures of phases, allowing to reproduce each spectrum with a definite number of abstract components (without a necessarily physical sense) obtained from linear combinations of the original spectra. The minimum number of necessary abstract components to reproduce the original spectra is directly correlated with the number of real components (number of different chemical environments) that are found in the assembly of analyzed data.

On the other hand, since the structure of the XANES spectra is mainly related with the local order of the absorbent element (Mn in the present case), the analysis of the XANES spectra allows to obtain electronic and structural information from specific atoms in non-crystalline phases, even at diluted conditions, which in general cannot be possible by XRD experiment. In terms of the PCA method, given an appropriate assembly of reference spectra, it is possible to determine if the sites of Mn in the standard compounds are also present at the set of the first analyzed data (target transformation). The details of the PCA analysis and the employed numerical procedures are already published elsewhere [20,21].

The EXAFS analyses were utilized for a qualitatively determination, from its Fourier transformation, of the radial distribution of elements in the environment of the Mn atoms.

### 2.4. Catalytic activity

Catalytic tests were carried out at atmospheric pressure in a continuous flow tubular glass reactor with 0.200 g of catalysts. The activity measurements were performed at the temperature range 100–300 °C. Ethanol was introduced to the reactor by a carrying gas of air flow through a saturator maintained at −2 °C. The concentration of ethanol in the feed was 300 ppm and the total gas flow was 20 $cm^3$ $min^{-1}$.

The reactants and reaction products were analyzed using on-line gas chromatograph (Shimadzu GC 8A) equipped with thermal conductivity detector. The analysis of ethanol, acetaldehyde and $CO_2$ was conducted through a Porapack T column.

## 3. Results and discussion

The BET specific surface areas of the manganese samples are listed in Table 1. EMD samples have the highest surface area, but the g-$MnO_2$ and the oxides obtained by decomposition of $KMnO_4$ (MnK and KMn) have a surface area much higher than the β-$MnO_2$ and $Mn_2O_3$.

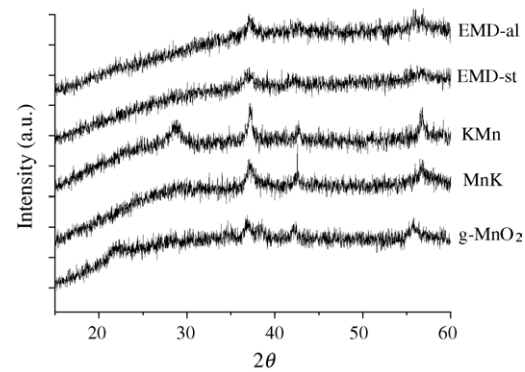


Fig. 2. X-ray powder diffraction patterns of the manganese oxides: g-$MnO_2$, MnK, KMn, EMD-st and EMD-al.

$MnO_2$ exists in various polymorphous modifications and they are usually noted $T(n,m)$ where $n$ and $m$ stand for the dimensions of the tunnels in the two directions perpendicular to the chains of edge-sharing octahedral. In this notation, pyrolusite and ramsdellite are denoted $T(1,1)$ and $T(1,2)$, respectively. Nsutite or γ-$MnO_2$ could be described as an irregular intergrowth of elements of ramsdellite and pyrolusite, thus the notation would be $T(1,1)$–$T(1,2)$.

Data from XRD indicated the presence of β-$MnO_2$ or pyrolusite phase (JCPDS 24-0735) for the commercial manganese dioxide and a well-crystallized α-$Mn_2O_3$ (JCPDS 41-1442) for the synthesized $Mn_2O_3$.

Fig. 2 shows the XRD powder patterns of the rest of the manganese samples. It can be seen that in general all the oxides have poorly resolved diffraction pattern indicating a low degree of crystallinity, in agreement with Chabre and Pannetier [9].

The XRD patterns of g-$MnO_2$ sample display low peaks at 22°, 37°, 38°, 42° and 56°, accounting to a γ-$MnO_2$ phase (JCPDS 17-0510). MnK and KMn present rather similar patterns except that the peak at $2\theta = 28°$ in the KMn pattern is missing in the MnK spectrum. These oxides may present the cryptomelane phase or α-$MnO_2$, which has a structure based on double chains of edge-sharing [$MnO_6$] octahedral forming [2 × 2] tunnels, so their notation is $T(2,2)$. This phase is usually obtained through reduction of $KMnO_4$ [22] and it is considered that $K^+$ is responsible for the stabilization of the structure. Some of the $Mn^{4+}$ cations are replaced by vacancies. Finally, both electrochemically deposited manganese dioxides (EMD-st and EMD-al) present a similar diffraction pattern again characterized by tiny peaks at 37, 42 and 56 °C. Note that the peak of 22°, characteristic of the γ-$MnO_2$, is missing in these two oxides. As we mentioned in the introduction, the great variety of γ-$MnO_2$ diffraction patterns reported (no fewer than 14) and the poor definition of its spectra because the low crystalline nature of them, make difficult the characterization of these phases by XRD. In addition, similar XRD peak positions are

present in both ramsdellite and pyrolusite due to reflections at different planes. Thanks to its characteristics, X-ray absorption spectroscopy results particularly appropriated for a more accurate characterization of these oxides and the nature of Mn-sites.

In effect, XANES can provide information on local atomic and local electronic structures. The Mn K-edge XANES employed as a characterization tool in this work, concerned to the dipole transition of the 1s core-hole electron to the p-like unoccupied projected density of states (DOS) at the Mn absorbing site. Since the 4p Mn states are strongly hybridized with O 2p and Mn 3d states of the neighboring atoms, the local p-like projected density of states is very sensitive to the charge distribution and local distortions of Mn–O bonds, as well as to any variations in Mn 3d–O 2p hybridization that is assumed to form the electronic states near the Fermi level [23].

The Mn K-edge XANES spectra of the references and sample compounds are present in Fig. 3a and b. They were used for subsequent analyses on the average oxidation state of Mn in each case and for determining the local structural characteristics of the Mn sites present in the different oxides.

In general, for Mn-compounds, a single pre-edge peak around 6542 eV in the XANES spectra indicates that Mn atoms occupy sites without a center of inversion. A simple inspection of Fig. 3 indicates that the Mn are preferably located on octahedral sites because the peak intensity in XANES spectra of the samples shown in that figure are much lower than in systems with a regular [$MnO_4$] species where Mn atoms are tetrahedrally coordinated [24].

As we can observe the procedures to obtain the MnK and KMn samples provide, in principle, the same crystallographic sites for the Mn. The corresponding spectra to the samples g-$MnO_2$, EMD-st and EMD-al have the same pattern, i.e., they would contain approximately the same type and concentration of Mn sites. As was already mentioned in Section 2, the electronic characteristics of the Mn atoms in each sample can be obtained by means of the analysis of the Mn K-edge shifting in XANES spectra. In principle, it is possible to obtain a quantitative estimation, averaged for all the Mn atoms in the sample, for the Mn oxidation state. Each different chemical species of Mn contribute to the experimental spectrum with its specific weight (relative concentration). The energy shifts on the absorption edge are directly related with the average oxidation state of the absorbent atom [18]. The absorption edge corresponding at $Mn^{3+}$ are at smaller energies than the corresponding one for $Mn^{4+}$. The origin of this shift is given by the different shielding effect that produces the valence electrons on the core electronic levels. When a valence electron is eliminated, the electron attached to the core level of the atom remains strongly bonded and this effect explains the larger energy necessary to remove it. In order to make a quantitative determination for the oxidation state (averaged for all the Mn atoms), we used the method described by Wong et al. for vanadium in vanadium oxides [18]. As it is shown in his work, all bound electronic transitions display a nearly linear relationship between their energy positions and formal oxidation state in the series of chemically similar Mn-compounds, e.g., oxides. This linear correlation is, however, normally measured at the inflection point of the edge (i.e., the edge position). Reference compounds (in our case metallic Mn, MnO, $Mn_2O_3$ and β-$MnO_2$) were employed to determine the energy shift of the absorption

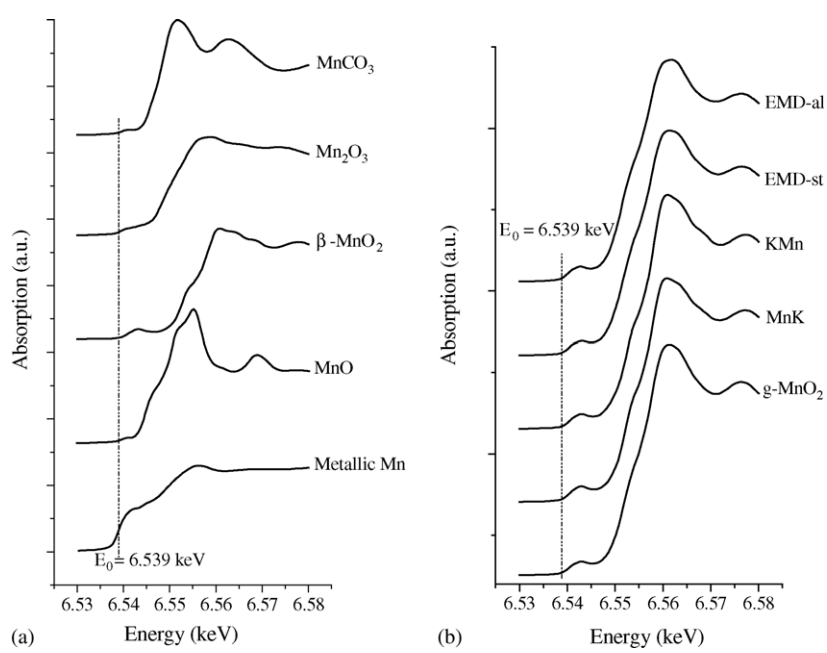


Fig. 3. (a and b) XANES spectra in the Mn K-edge region of several manganese samples and references: metallic Mn, MnO, $Mn_2O_3$, β-$MnO_2$, $MnCO_3$, g-$MnO_2$, MnK, KMn, EMD-st and EMD-al.

Table 2
Energy shift and mean oxidation state of the reference compounds and samples the errors are indicated by sub index

| References and samples | Energy shift $E - E_0$ (eV) | Mn mean oxidation state |
|---|---|---|
| Metallic Mn | $0_1$ | 0 |
| MnO | $6_1$ | 2 |
| $Mn_2O_3$ | $9_1$ | 3 |
| β-$MnO_2$ | $14_1$ | 4 |
| g-$MnO_2$ | 12.9 | $3.9_7$ |
| MnK | 13.3 | $4.0_7$ |
| KMn | 13.3 | $4.0_7$ |
| EMD-st | 12.9 | $3.9_7$ |
| EMD-al | 12.6 | $3.8_7$ |

K-edge for different formal oxidation states. The obtained average oxidation state for Mn in each sample is shown in Table 2 and Fig. 4. Even this determination is not precise enough because the error in the energy resolution at Mn K-edge (see horizontal bars in Fig. 4) is sufficient for a qualitative description of the trend of the mean oxidation state of Mn in Mn-species present in different catalysts.

PCA analysis, employing a program in a FORTRAN code, was carried out to determine the number and the nature of all the different Mn sites present in the set of samples. This analysis, excluding the reference compounds, indicates that there are three principal components. Therefore, it is possible to reproduce, with acceptable accuracy considering the confidence parameter of the method [20], the XANES spectra for: $Mn_2O_3$, β-$MnO_2$, g-$MnO_2$, MnK, KMn, EMD-st and EMD-al by the linear superimposition of only three spectra (abstract components). The residue of the obtained components contributes to the total signal lower than the experimental noise level. This can be clearly visualized through the amplitude of the components that appear in Fig. 5. This means, in terms of the material composition, that the PCA approximation is valid and there are only three distinguishable chemical environments for the Mn. One of the three environments proposed for the Mn, should correspond to Mn in β-$MnO_2$. This analysis was possible by means of the target transformation (TT) routine, present

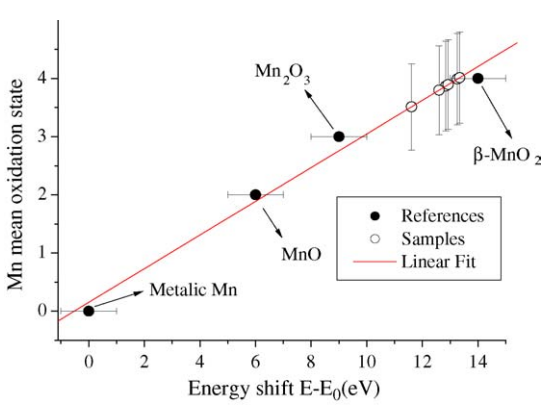


Fig. 4. Oxidation state determination of Mn-compounds by employing of the Mn K-edge the energy shift according to the Wong's method.

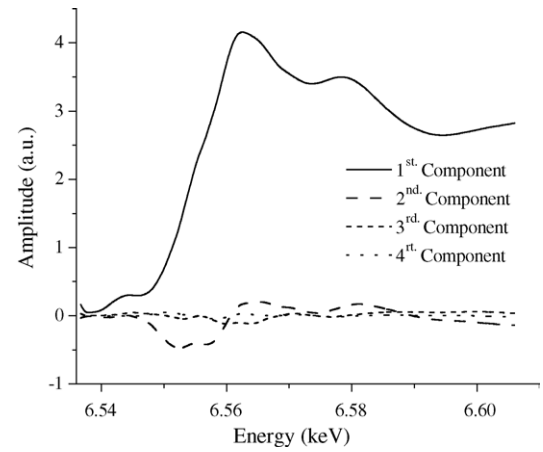


Fig. 5. Abstract components obtained by PCA analysis.

in the PCA program. By TT routine it is possible to determine if a pure (XANES) spectrum, corresponding to one of the reference compounds, can be reproduced from the main components that reproduce the experimental assembly of data. In case of not being able to reproduce reference compound spectrum with the same principal components previously determined by PCA, it is possible to assert then that the sites of this compound (all of them) are not present in the assembly of analyzed data. With this routine we can show that the sample g-$MnO_2$ is also reproduced through the same set of principal components. Taking into account this result and that the g-$MnO_2$ XANES spectrum has a similar pattern than the γ-$MnO_2$ or nsutite ones, we can infer that the other site corresponds to the ramsdellite structure.

Fig. 6 shows the Fourier transform (FT) of the oscillation EXAFS for the pyrolusite and the nsutite. Considering a single scattering model for the photoelectrons, the first peak in the FT spectra is due to the first oxygen atoms with octahedral symmetry, the second one was previously associated with the presence of the first cationic neighbors and the third one to the second cationic neighbors [25].

As it was previously discussed in Ref. [10], the higher intensity for the second Mn–Mn shell (at ∼3.4 Å, see vertical line in Fig. 6) in pyrolusite sample evidence the higher mean coordination number of Mn at the second cationic coordination shell. One possible explanation for this difference can be supported by the hypothesis of the presence of Mn vacancies in the nsutite compound. It is important to note that the rest of the samples (catalysts) have similar Fourier spectra of the nsutite one. This fact is also consistent with the mean oxidation state lower than 4+ determined by XANES for Mn in those samples.

In short, from the EXAFS and XANES results we can suppose that the third site of Mn is associated to the presence of nsutite-like compounds and corresponds to Mn in octahedral environment of oxygen atoms with vacancies of Mn in the second cationic shell of coordination, decreasing then the formal oxidation state of Mn by charge balance.

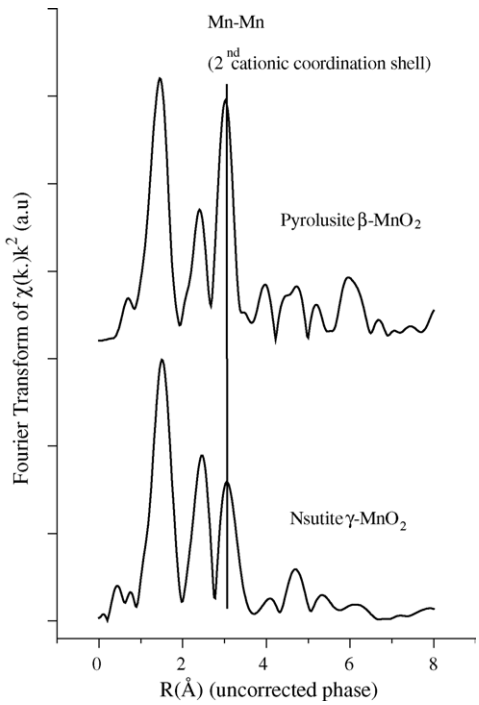


Fig. 6. Fourier transform (FT) of the oscillation EXAFS for the pyrolusite and the nsutite.

### 3.1. Catalytic activity

Some of the catalysts were tested in the reaction of complete oxidation of ethanol to $CO_2$ and $H_2O$. The ignition curves are plotted in Fig. 7. It can be seen that the two synthetic oxides tested (g-$MnO_2$ and MnK) have a similar activity, characterized by a temperature at which the conversion is 50% ($T_{50}$) of approximately 150 °C. At 200 °C, the conversion of ethanol is total and the selectivity to $CO_2$ reaches the 100% for both oxides. They present a higher activity than $Mn_2O_3$ and β-$MnO_2$, which have a $T_{50}$ of 180 and 250 °C, respectively. The best activity of these catalysts compared with $Mn_2O_3$ and $MnO_2$ could be

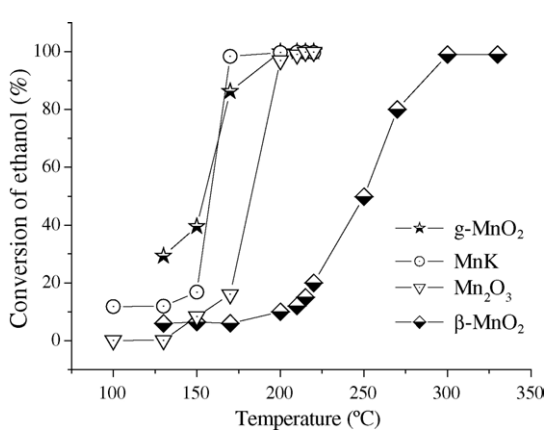


Fig. 7. Total ethanol conversion as a function of temperature: g-$MnO_2$, MnK, $Mn_2O_3$ and β-$MnO_2$.

attributed to the presence of $Mn^{4+}$ and $Mn^{3+}$ species (detected by XANES) and to the existence of $Mn^{4+}$ vacancies (evidenced by EXAFS results), which generates OH species. These factors lead to a high electrical conductivity [9], and as it was pointed out by Volkenshtein in the ''The Electronic Theory of Catalysis'' [26], the more the electronic conductivity, the more the catalytic properties of the solid. Besides, an increase in the catalytic behavior of manganese oxides with the decrease of the crystallinity was observed by Shareen and Selim [27].

## 4. Conclusions

Among the different techniques of synthesis, a series of nanocrystalline Mn oxides was prepared; they were structurally and electronically characterized by means of the XRD, XANES and EXAFS techniques. The obtained results allow us to conclude the following:

(1) The obtained oxides of manganese present a very poor crystalline structure independently from the employed synthesis.
(2) The mean oxidation state value of all the samples is between 3+ and 4+. This fact is in agreement with the presence of cationic vacancies in synthesized Mn-oxide samples.
(3) As shown by PCA, the Mn is present in three different environments. One of the octahedral sites in the synthesized samples is similar to the Mn site present in the pyrolusite (β-$MnO_2$). In agreement with preliminary EXAFS results, a second site should correspond to the presence of ramsdellite phase while the third site can be associated with an octahedral Mn-site.
(4) For the second Mn-site described above, the second Mn–Mn coordination shell is lower than the corresponding one for nsutite. This can be associated with presence of Mn-vacancies, which should reduce the mean Mn formal oxidation state by charge balance as can be also observed by XANES.
(5) The synthesized manganese-based oxides are active catalysts for the total oxidation of ethanol. The catalytic activity is related, on one hand, to the presence of the $Mn^{3+}$–$Mn^{4+}$ couple and $Mn^{4+}$ vacancies, which generates OH groups, and on the other to the low crystalline structure of the oxides.

## Acknowledgements

M.A.P. and S.J.A.F. thanks to the CICpBA for the scholarship offered for the execution of this work. The work has been supported by the Brazilian Synchrotron Light Source (LNLS, Campinas, Brazil) under proposal D04B-XAS1-1889 and CONICET, CICpBA, Fundación Antorchas

under Project 14116-120 and ANPCYT under grant PICT 06-17492 (Argentina).

## References

[1] M. Paulis, L. Ganda, A. Gil, J. Sambeth, J. Odriozola, M. Montes, Appl. Catal. B 26 (2000) 37.
[2] V. Bentrup, A. Bruickner, M. Ritcher, R. Fricke, Appl. Catal B 32 (2001) 229.
[3] M. Peluso, J. Sambeth, H. Thomas, React. Kinet. Catal. Lett. 80 (2003) 241.
[4] M. Álvarez-Galván, V. de la Peña O'Shea, J. Fierro, P. Arias, Catal. Commun. 4 (2003) 223.
[5] L. Gandía, M. Vicente, A. Gil, Appl. Catal. B 38 (2002) 295.
[6] Y. Liu, M. Luo, Z. Wei, Q. Xin, P. Ying, C. Li, Appl. Catal. B 29 (2001) 61.
[7] Y. Liu, Z. Wei, Z. feng, M. Luo, P. Ying, C. Li, J. Catal. 202 (2001) 200.
[8] F. Arena, T. Torre, C. Raimondo, A. Parmalina, Phys. Chem. Chem. Phys. 3 (2001) 1417.
[9] Y. Chabre, J. Pannetier, Prog. Solid State Chem. 23 (1995) 1.
[10] F. Petit, J. Dürr, M. Lenglet, B. Hannoyer, Mater. Res. Bull. 28 (1993) 959.
[11] C. Lahousse, A. Bernier, P. Grange, B. Delmon, P. Papaefthmiou, T. Ionnides, X. Verykios, J. Catal. 178 (1998) 214.
[12] A. Ibarra-Palos, P. Strobel, O. Proux, J. Aceman, M. Anne, M. Morcrette, Electrochim. Acta 47 (2002) 3171.
[13] S. Randall, D. Sherman, K.V. Ragnarsdottir, Chem. Geol. 151 (1998) 95.
[14] G. Pan, Y. Qin, X. Li, T. Hu, Z. Wu, Y. Xie, J. Colloid Interface Sci. 271 (2004) 28.
[15] Join Committee on Powder Diffraction Standards, JCPDS Files, International Center for Diffraction Data, 2000.
[16] A. Ramos, Y. Tolentino, H., Alves, M.C.M., Energy Resolution at LNLS-XAS beam line MeT-02/99, 1999.
[17] B.K. Teo, EXAFS: basic principles and data analysis, in: Inorganic Chemistry Concepts, vol. 9, Springer-Verlag, Berlin, 1986.
[18] J. Wong, F.W. Lytle, R.P. Messner, D.H. Maylotte, Phys. Rev. B 30 (1984) 5596.
[19] E.R. Malinowski, D.G. y Howery, Factor Analysis in Chemistry, Wiley, New York, 1980.
[20] M. Fernández-García, C. Márquez, G.L. Haller, J. Phys. Chem. 99 (1995) 12565.
[21] T. Ressler, J. Wong, J. Roos, I.L. Smith, Environ. Sci. Technol. 34 (6) (2000) 950–958.
[22] H. Kim, J. Kim, S. Oh, Chem. Mater. 11 (1999) 557.
[23] F. De Groot, Coord. Chem. Rev. 249 (2005) 31–63.
[24] A. Bianconi, J. Garcia, M. Benfatto, A. Marcelli, C.R. Natoli, M.F. Ruiz-Lopez, Phys. Rev. B 43 (1991) 6885.
[25] A. Manceau, J.M. Combes, Phys. Chem. Miner. 15 (1988) 283.
[26] F. Volkenshtein, The Electronic Theory of Catalysis on Semiconductors, Pergamon Press, New York, 1963.
[27] W. Shareen, M. Selim, Thermochim. Acta 332 (1998) 117.